ENCLOSURE 2
ATTACHMENT 6

SHINE MEDICAL TECHNOLOGIES, INC.

SHINE MEDICAL TECHNOLOGIES, INC. APPLICATION FOR CONSTRUCTION PERMIT
RESPONSE TO REQUEST FOR ADDITIONAL INFORMATION

ANL/CSE-13/38
FY13 PROGRESS REPORT ON THE PHASE I MINI-SHINE WATER IRRADIATIONS AND MICRO-SHINE IRRADIATIONS

34 pages follow

CONTENTS

FIGURES

FIGURES (Cont.)

FIGURES (Cont.)

TABLES

FY13 PROGRESS REPORT ON THE PHASE I MINI-SHINE WATER IRRADIATIONS AND MICRO-SHINE IRRADIATIONS

1 INTRODUCTION

Five liters of water have been irradiated at Argonne's electron linac nine different times as part of the mini-SHINE/micro-SHINE experiments. Irradiation of samples is performed by impinging the linac electron beam on a tantalum target, which is located in a dry well of the target vessel holding the 5 L target solution. Neutrons and high-energy x-rays are produced, which leads to the radiolysis of water. Radiolysis produces many radicals in the water, which ultimately leads to the formation of peroxide, hydrogen (H_2), and oxygen (O_2). Irradiations lasted for 15–120 minutes with water continuously circulated, at 40 mL/min, through the target solution monitoring loop (TSML). The TSML includes a pH electrode, conductivity cell, and a turbidity sensor. The in-line measurements are collected using a data-acquisition and remote-control program written in the National Instruments LabVIEW development environment. The control functionality of the program allows remote operation of the solenoid valves used in the mini-SHINE ^{99}Mo remote recovery system. Progress and development of the target solution monitoring glovebox and its components (valves, pH electrode, conductivity cell, turbidity cell, shielding, etc.) will be discussed as well. Gases were continuously monitored using a combination of a residual gas analyzer (RGA) and a gas chromatograph (GC) equipped with a mass spectrometer (MS) and thermal conductivity detector (TCD) and passed through a catalytic converter (catalyst supplied by Ford Motor Company) to recombine the hydrogen and oxygen.

During each water irradiation, two dry wells in the target solution vessel tank lid were utilized to perform micro-SHINE experiments. In a typical micro-SHINE experiment, 2 mL of solution (water, sodium bisulfate, or uranyl sulfate [0.22–93% U-235]) were irradiated in a closed quartz vial containing 0.8–1.0 g Pt/alumina H_2-O_2 recombination catalyst to recombine the H_2 and O_2 generated during radiolysis. Using a metal basket to hold the Pt catalyst was the best way to minimize solution loss, but appears that the micro-SHINE solutions bubbled during irradiation because the catalyst was wetted by the micro-SHINE solutions. Each quartz vial was kept in a secondary aluminum container during irradiation. The pressure in each quartz vial was measured post-irradiation by inserting a needle, connected to a manometer, through the rubber septum. The pH of each micro-SHINE solution was measured post-irradiation as well.

The original goal of the micro-SHINE experiments was to confirm that precipitation of uranyl peroxide can be prevented by adding a catalyst such as $FeSO_4$ to destroy peroxide. After successfully demonstrating that $FeSO_4$ is an effective catalyst for peroxide destruction, subsequent micro-SHINE solutions were used as tracers to perform a Mo-separation and recovery column experiment, a sulfate-to-nitrate conversion, and iodine speciation experiments.

Table 1 shows the water irradiations and micro-SHINE irradiations that have been performed in Fiscal Year 2013 (FY13).

TABLE 1 Water and Micro-SHINE Irradiations Performed in FY13

Date of Irradiation	Mini-SHINE	Micro-SHINE #1 (Position #1)	Micro-SHINE #2 (Position #2)
07/26/13	H_2O	H_2O	
07/30/13	H_2O	0.55 M $NaHSO_4$ 3×10^{-3} mM stable Mo	1.26 M $NaNO_3$ 4.5×10^{-3} mM stable Mo
07/31/13	H_2O	130 g-U/L UO_2SO_4 DU 10 ppm $FeSO_4$	130 g-U/L UO_2SO_4 DU no H_2O_2 catalyst
08/01/13	H_2O	130 g-U/L UO_2SO_4 LEU 1 ppm $FeSO_4$	130 g-U/L UO_2SO_4 LEU 10 ppm $FeSO_4$
08/19/13	H_2O	~130 g-U/L UO_2SO_4 (LEU) 1 ppm Fe SO_4	~130 g-U/L UO_2SO_4 (LEU) 1 ppm Fe SO_4
08/20/13	H_2O	~130 g-U/L UO_2SO_4 (HEU) 1 ppm Fe SO_4	~130 g-U/L $UO_2(NO_3)_2$ (HEU)
09/03/13	H_2O	~130 g-U/L UO_2SO_4 (LEU) 1 ppm Fe SO_4	~130 g-U/L UO_2SO_4 (HEU) 1 ppm Fe SO_4
09/11/13	H_2O	~130 g-U/L UO_2SO_4 (HEU) 1 ppm Fe SO_4	~130 g-U/L UO_2SO_4 (HEU) 1 ppm $FeSO_4$
09/24/13	H_2O	~130 g-U/L UO_2SO_4 (HEU) 1 ppm Fe SO_4	~130 g-U/L UO_2SO_4 (HEU) 1 ppm $FeSO_4$

2 TSML RESULTS

The TSML and Mo-recovery gloveboxes were set up and installed during the third and fourth quarters of FY13. This section describes the activities completed in FY13 that led to the installation and testing of the TSML system. The remotely operated Mo-recovery system is described in a separate report.

2.1 VAN DE GRAAFF TESTING

All components were tested using the Argonne National Laboratory (Argonne) 3.0-MeV Van de Graaff electron accelerator prior to installation. High-energy x-rays were produced by impinging the 3.0-MeV electron beam on a tungsten converter. Components were irradiated for at least 48 hours. Testing of components began with several solenoid valves during the first quarter of Fiscal Year 2012 (FY12). The solenoid valves were then down-selected to a Peter Paul direct acting valve (Figure 1). The valve had been tested with 1 M HNO_3 in the second quarter of FY12. Testing of this valve with 1 M H_2SO_4 in the first quarter of FY13 resulted in significant corrosion of the plunger (Figure 2). The body of the solenoid valve is 316SS. However, the

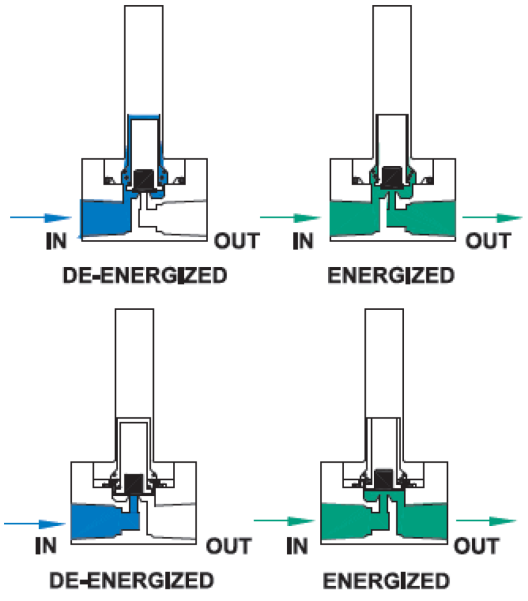

FIGURE 1 Diagram Showing Interior Portions of Solenoid Valves That Come into Contact with the Process Fluid: Direct-Acting Solenoid Valve (top) and Isolation Solenoid Valve (bottom) (isolation solenoid valve constructed to prevent process fluid from contacting plunger [piston])

FIGURE 2 Interior of the Irradiated Peter Paul Direct-Acting Solenoid Valve (Top left: Plunger [piston] and outer assembly showing the spring that holds pressure on the plunger to maintain a seal between the rubber insert and the orifice. Top right: Magnified view of the tip of the plunger with an arrow showing the interface between the rubber seal and plunger body. Bottom center: Body interior showing the orifice [center hole] that is sealed by the rubber seal on the plunger.)

plunger (piston) that is used to actuate the opening of the valve is made of 430FR stainless steel. The 430FR stainless steel is a ferritic chromium-iron alloy specially developed for soft magnetic components that must operate in corrosive environments (Carpenter 2004). Although 430FR stainless steel has good corrosion resistance to nitric acid, it has restricted use with sulfuric and phosphoric acids (Carpenter 2004). The butyl rubber insert in the end of the plunger retained structural integrity and was not significantly affected by the H_2SO_4 (Figure 2). The corrosion of the 430FR plunger resulted in the dissolved material plating out on the surface of the 316SS body. This deposition of material significantly affected the surface near the orifice, impeding formation of a proper seal between the butyl rubber insert and the orifice edge.

When energized, the solenoid coil (magnetic coil) draws the plunger up, thus opening the valve and allowing fluid flow. The process fluid can come into contact with the plunger with this type of valve. A spring is used to maintain pressure on the plunger against the orifice in the closed position. In an isolation solenoid valve, a diaphragm is mounted in a fashion that prevents the process fluid from contacting the plunger (Figure 1). A spring is used to maintain pressure on the plunger against the orifice to close the valve. Failure of the diaphragm in the isolation valve would result in the process fluid coming into contact with the plunger material.

A new valve was selected in the mid-first quarter of FY13 and tested in late first quarter of FY13. The valve (Figure 3) is a Gems Sensors AS series isolation solenoid valve (p/n AS2015-1-SB5-E-C204). The valve has a 316SS body and an ethylene-propylene copolymer (EPR) diaphragm. Testing of the valve after exposure to the radiation field of the Argonne Van de Graaff accelerator was successful. Forty new valves were received late in the second quarter of FY13.

2.2 IMPLEMENTATION OF TSML FLOW DIAGRAM

The flow diagram for the TSML system is shown in Figure 4. Implementation of the flow diagram into the TSML glovebox is shown in Figure 5. A single positive displacement pump

FIGURE 3 Gems Sensors AS Series Isolation Solenoid Valve (The EPR diaphragm keeps the plunger [piston] isolated from the process fluid.)

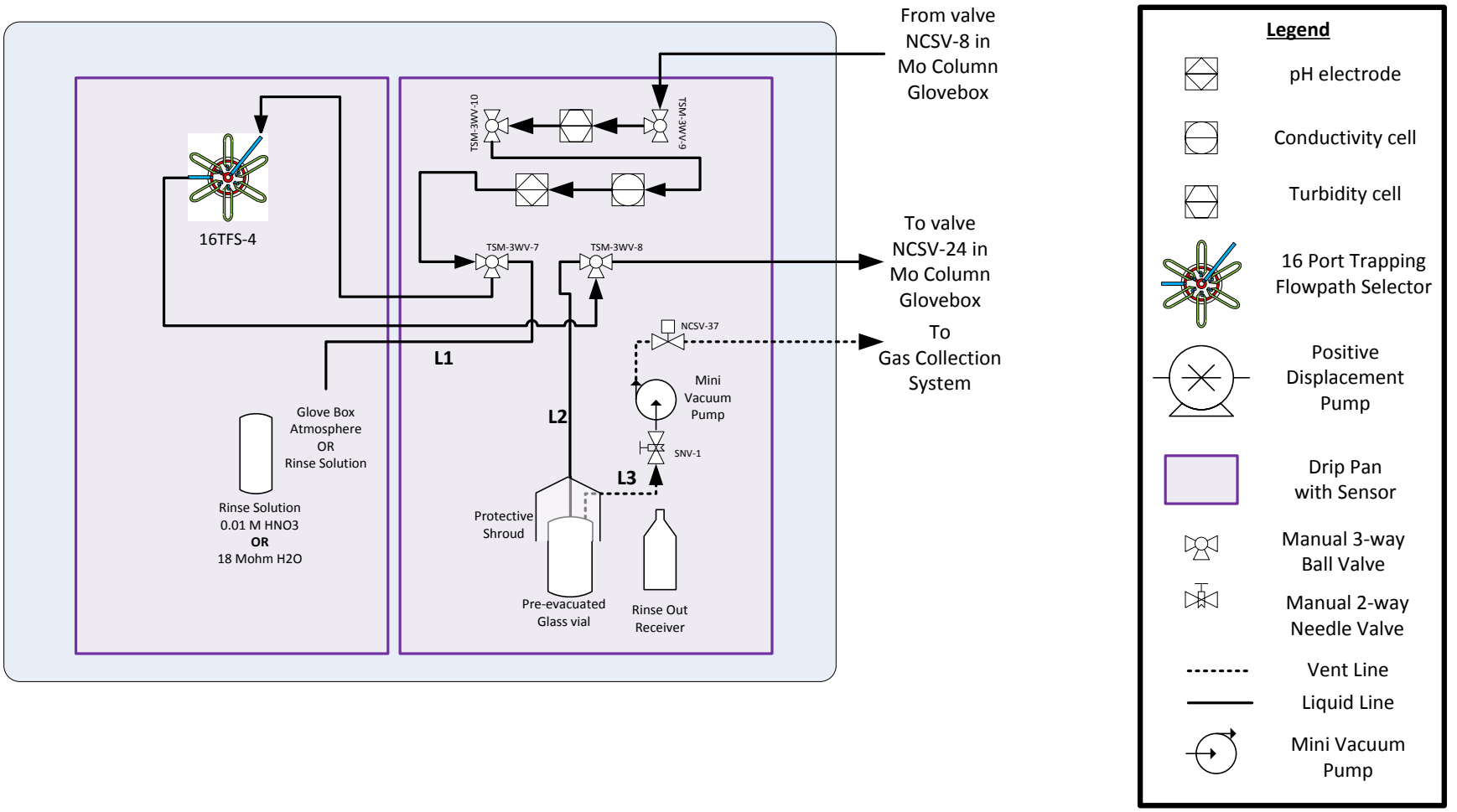

FIGURE 4 Flow Diagram for the TSML Glovebox

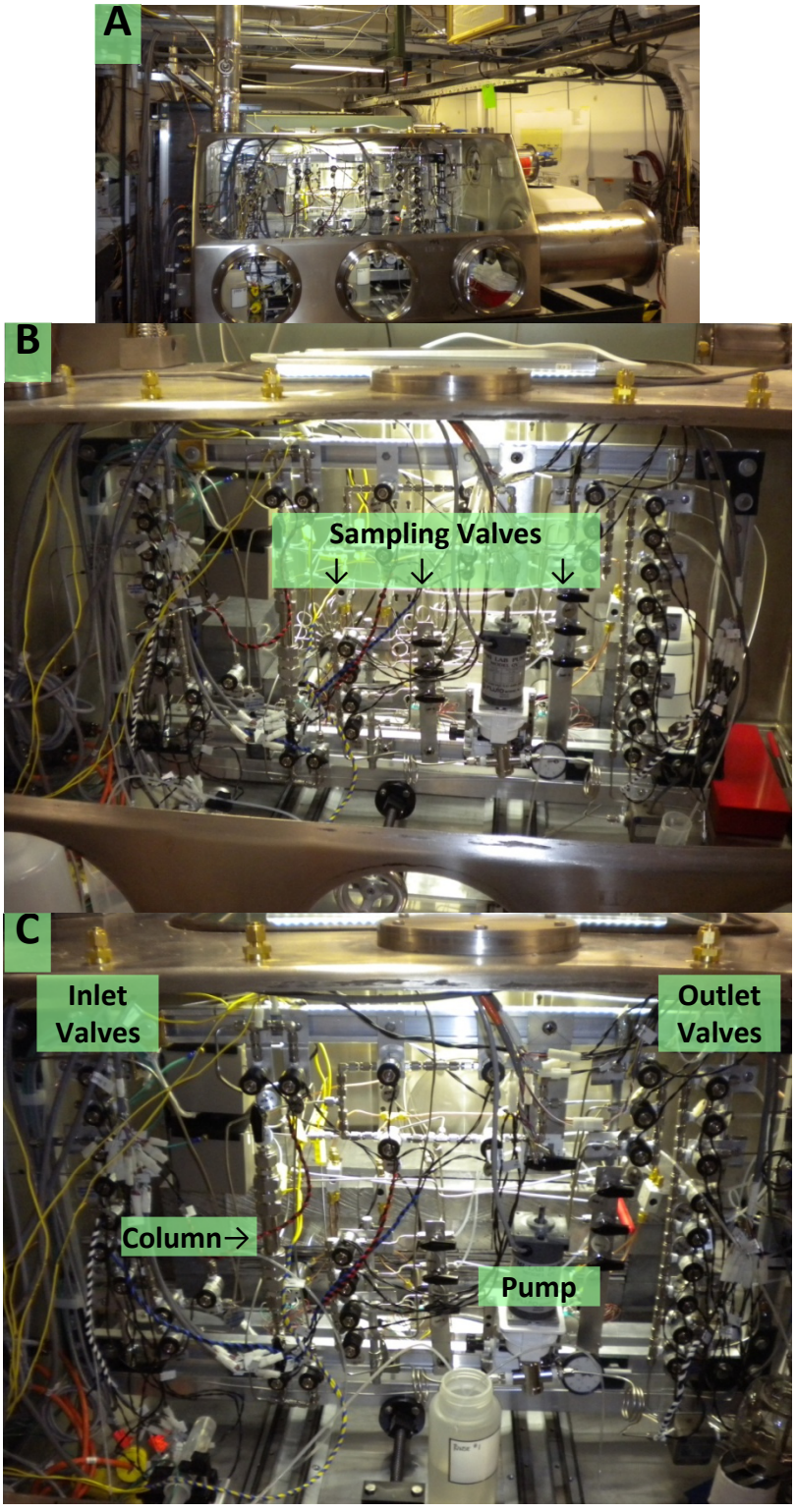

FIGURE 5 (A) Photos of the Mo-Recovery Glovebox and (B and C) the Remote-Controlled Equipment Installed in It (the three 16-loop trapping flow-path selector valves can be seen in B)

serves both the TSML and Mo-recovery systems. The pump resides in the Mo-recovery glovebox.

During target solution monitoring, the pump draws solution from the target vessel in the mini–hot cell. The solution first enters the Mo-recovery glovebox (Figure 6) at one of the inlet solenoid valves on the left-hand side. The target solution is then drawn over to the TSML glovebox. The solution passes through the turbidity cell, then the conductivity cell, then the pH electrode cell, then finally through a Valco Instruments Co., Inc., 16-loop trapping flowpath selector (TFS) sampling valve. The solution is then drawn back to the Mo-recovery glovebox and passes through the pump. After the pump, the solution is pushed through a liquid flow meter before exiting the Mo-recovery glovebox at one of the outlet solenoid valves (Figure 6) on the right-hand side as it is returned to the target vessel.

Samples are retreived from the TFS sampling valves using pre-evacuated vials that are sealed with a septum. The vacuum in the 10 mL vials has been shown to fully draw the solution samples over. To provide a means for retreiving the entirety of each sample and to clean the retrieval line between samples, a miniature vacuum pump was installed in each glovebox. The vacuum pump is connected to a solenoid valve to allow the exhaust from the pump to be vented to the gas collection system. Operation of the vacuum pump and solenoid valve is controlled through a single toggle switch mounted in the glove box. The vacuum pump system has proven to be very effective at withdrawing any residual liquid from the loops of sampling valve and to remove droplets from the sample retrieval lines.

2.3 LABVIEW SYSTEM

Programming of the LabVIEW system to remotely control all of the solenoid valves and capture process values began in the late second quarter of FY13. Control of the solenoid valves was accomplished in the early third quarter of FY13. Modifications to the data-acquistion and remote-control program have been made during the fourth quarter of FY13.

The system can be operated either in automated or manual mode. In manual mode, a user has full control of all of the liquid solenoid valves and the air-actuated sampling valves. During automated mode, the user simply presses the NEXT STEP button, seen on the right side of Figure 7. With each press of the button, the solenoid valves relevent to the current step in the process are opened and unnecessary valves are closed. The 24-VDC solenoid valves are controlled using quad-format solid-state relays from Measurement Computing Corporation. The area of the program that is used to control the three sampling valves is shown in Figure 8.

The program captures the temperatures of the upper and lower pre-heaters and the column. The system also records the conductivity, pH, and turbidity values. In addition, the program records the values of the load cells serving the dump tank and the pressure gauges in the gas collection system. All values are time-stamped. To facilitate documentation of an experimental run, several comment boxes are available for users to enter time-stamped comments.

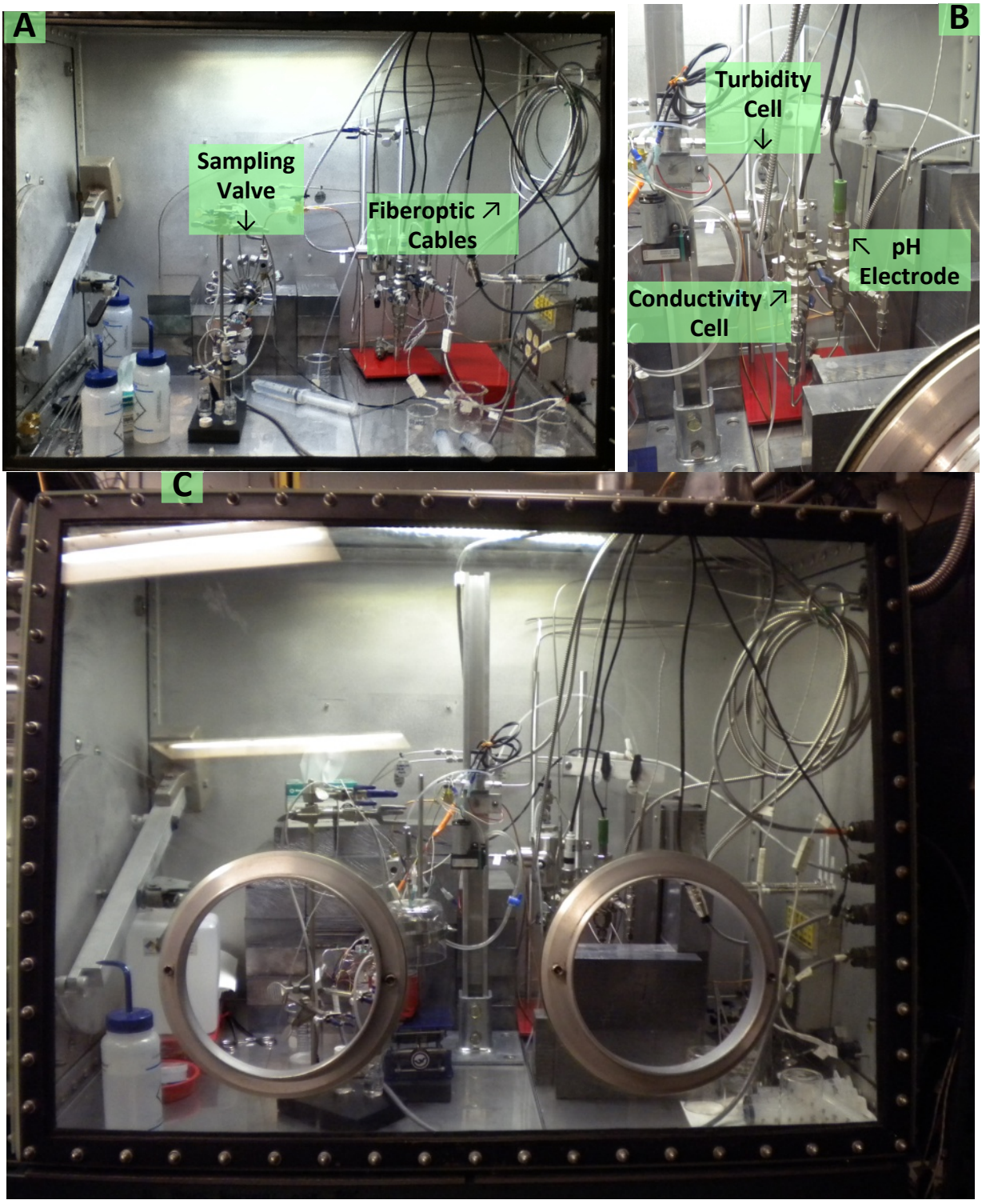

FIGURE 6 Photos of TSML Glovebox: (A) the 16-loop TFS; (B) the Turbidity Cell (Kemtrak), Conductivity Cell (Fisher Scientific), and pH Electrode (Hanna Instruments); (C) 16-loop TFS and the Probes Shielded by Lead Bricks (The miniature vacuum pump can be seen on the left side of photo [B].)

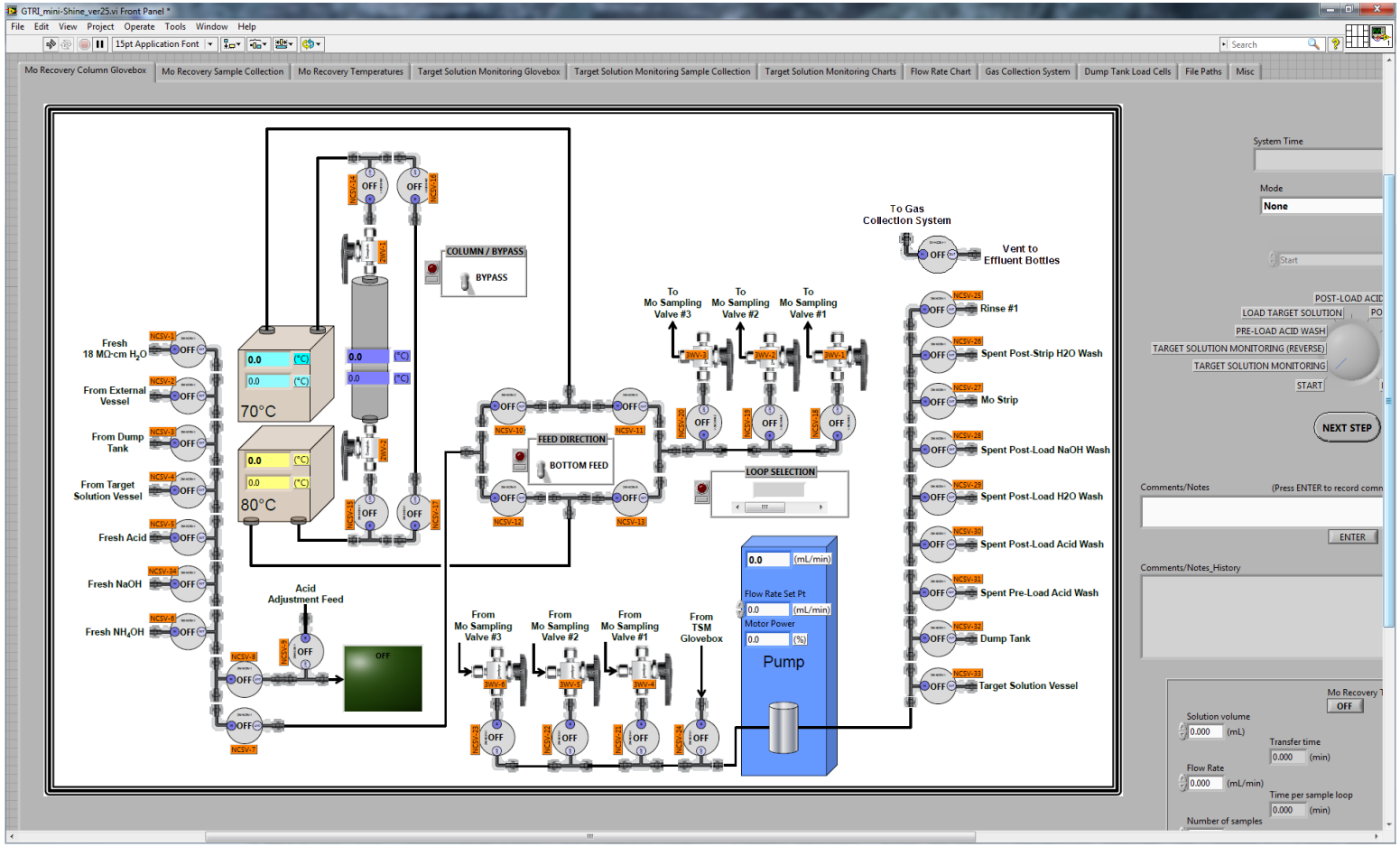

FIGURE 7 Screen Capture of the Data Acquisition and Remote Control Program Written in the LabVIEW Environment

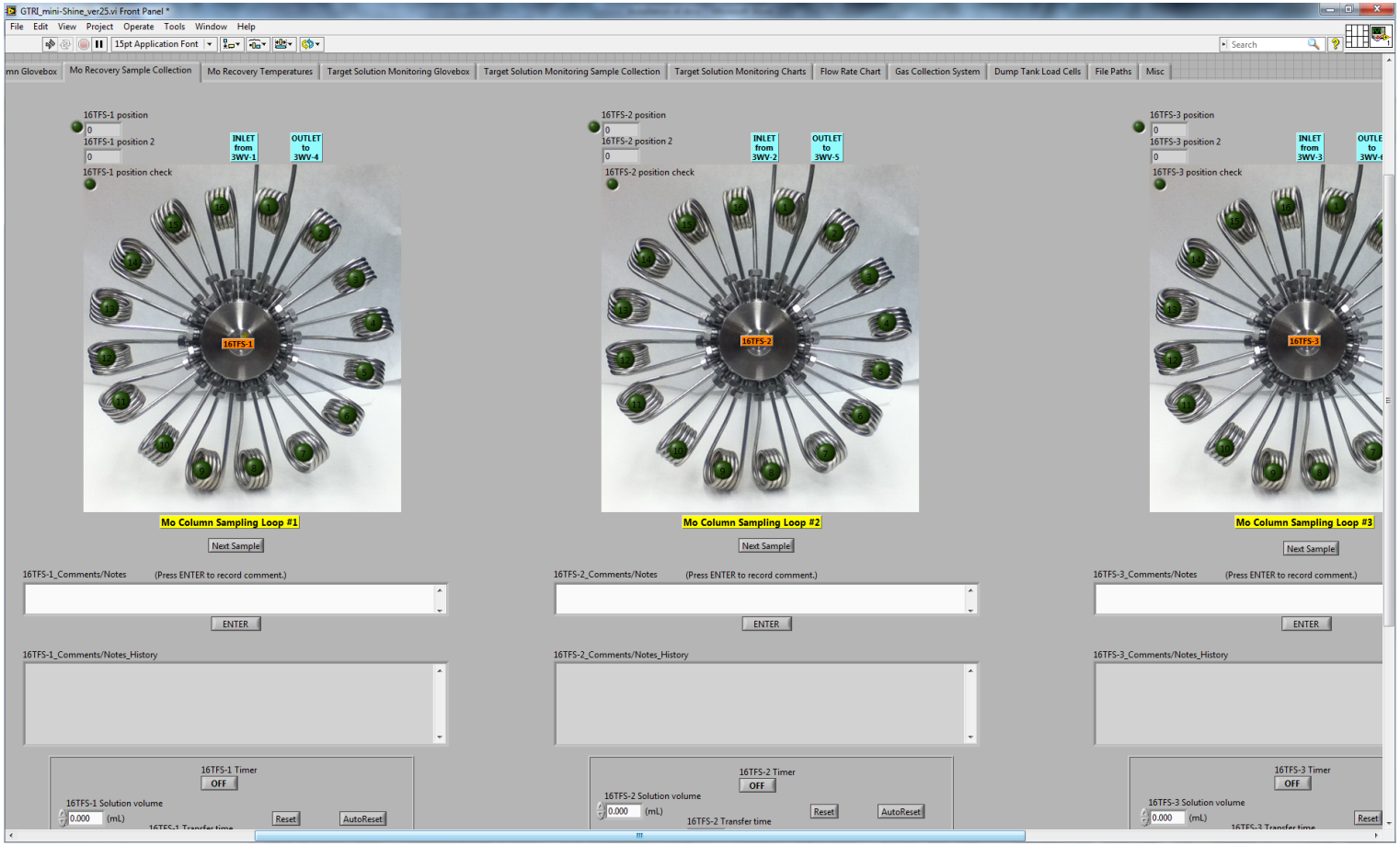

FIGURE 8 Screen Capture of the Program Tab That Is Used to Control the Mo-Recovery Sampling Valves

2.4 pH ELECTRODE AND CONDUCTIVITY CELL

Both the conductivity cell and the pH electrode operated normally during the nine mini-SHINE water runs. The conductivity cell and pH electrode were calibrated before every mini-SHINE water run. The deionized water in the target vessel was circulated at 40 mL/min through the TSML glovebox during the mini-SHINE water experiments. Conductivity and pH data from mini-SHINE runs 5 (Figure 9) and 8 (Figure 10) are shown below.

The conductivity cell from Fisher Scientific is a four-band cell with a cell constant of K = 1. The four-band cell has a better response and can be used over a wider range. The cell is interfaced to a Eutech Instruments alpha-CON2000P conductivity controller. Use of a cell with K = 1 is required for the low conductivity range of 0–2000 μS/cm used during the runs with water in the target vessel. A four-band cell with a cell constant of K = 10 will be required for the $NaHSO_4$ and UO_2SO_4 process solutions, because the conductivity range is expected to be on the order of 0–1000 mS/cm. The conductivity of 18 MΩ·cm deionized water is approximately 0.02–0.05 μS/cm. The conductivity controller is equipped with automatic temperature compensation (ATC). The controller is not reading the resistive temperature device (RTD) probe correctly, so the conductivity measurements are made at a fixed temperature of 25°C. The conductivity RTD probe is being read by a separate meter and being recorded to permit temperature correction of the conductivity at a later date.

The Hanna Instruments pH electrode is interfaced to a Eutech Instruments alpha-pH2000P controller. The controller is equipped with ATC so that the pH is properly temperature compensated. With water in the target vessel, the pH electrode was calibrated using off-the-shelf standards. During tests with either $NaHSO_4$ or UO_2SO_4, standards will have to be created at the high salt concentrations equivalent to the solutions to be used.

2.5 TURBIDITY CELL

The Kemtrak TC007 Turbidimeter/Controller resides outside of the radiation field because it is mounted to the rack that houses the LabVIEW data acquisition and control system. Both the light source and detectors are housed in the TC007. The unit uses a near-infrared (NIR) light source–high-power TS AlGaAs infrared LED lamp producing NIR light at a wavelength of 875 nm. The units for turbidity that are being used are the NTU (nephelometric turbidity units). The picture below (Figure 11) demonstrates the relation between NTU and the visual turbidity of a solution. The turbidity cell was calibrated with two standards (1 and 100 NTU).

Two components of the turbidity cell were tested at the Argonne 3.0 MeV Van de Graaff in the second quarter of FY12. Both the turbidity cell and a fiberoptic cable were irradiated for 48 h. The fiberoptic cable did not show any signs of signal degradation in the range of 875 nm when tested with a Avantes ultraviolet-visible (UV-vis) light source and detector. The turbidity cell remained leak-tight and was tested with the turbidimeter controller unit and remained operable. The 130 m, triple 600 μm core fiberoptic cable was installed in the late second quarter of FY13. The turbidity cell was installed in the TSML glovebox in the third quarter of FY13.

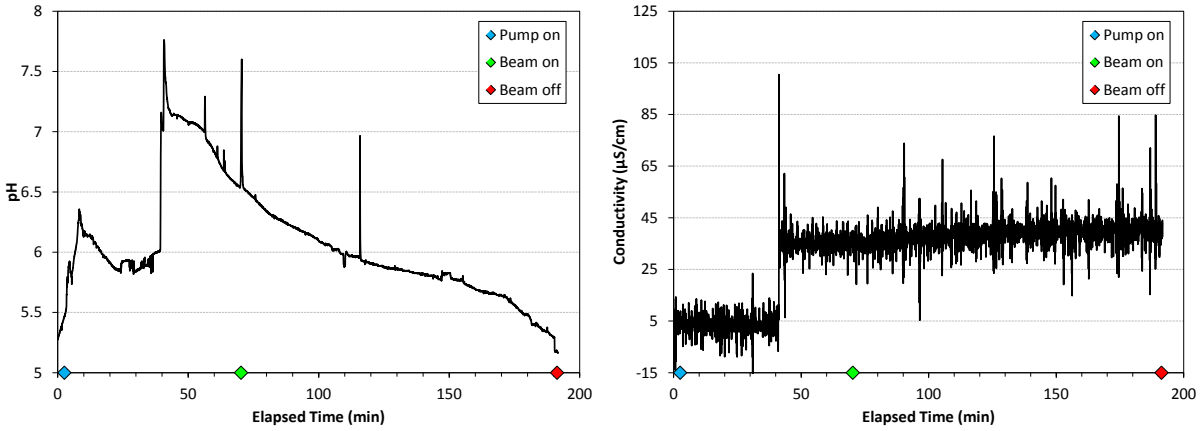

FIGURE 9 Plots of pH and Conductivity Values from Micro-SHINE Irradiation 5 Conducted on 8/19/2013 (No averaging of data has been performed.)

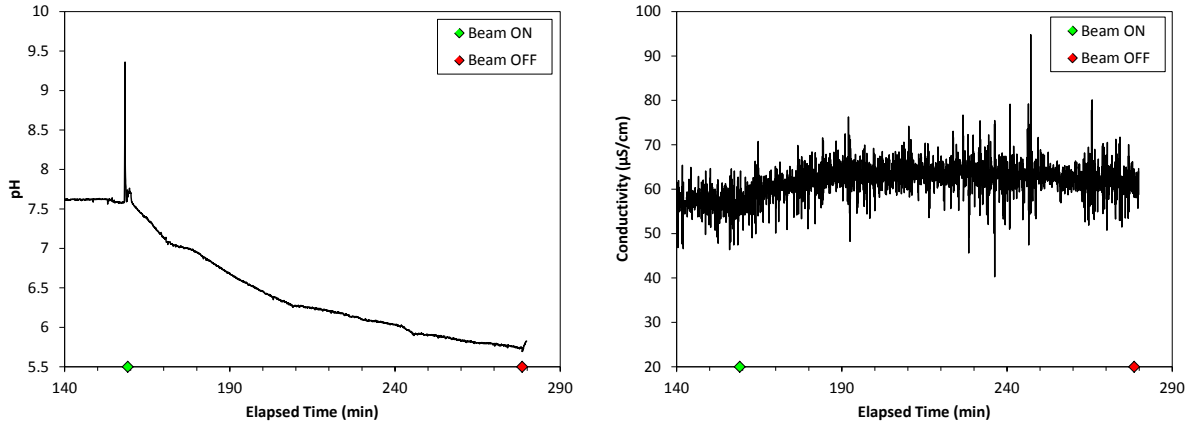

FIGURE 10 Plots of pH and Conductivity Values from the Micro-SHINE Irradiation 8 Conducted on 9/11/2013 (No averaging of data has been performed.)

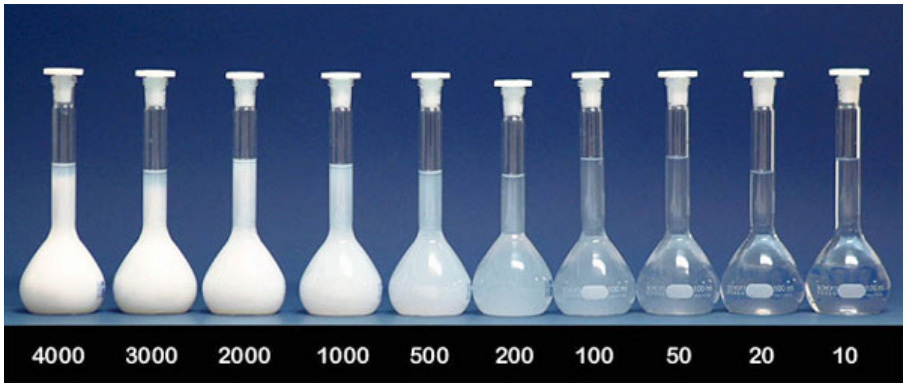

FIGURE 11 Photo Showing Relation to Visible Turbidity and NTU (see http://www.optek.com/Turbidity_Measurement_Units.asp)

Initially, the TSML glovebox was not shielded. The first test of the turbidity meter while in the presence of a 60-Hz electron beam (~3.5 kW) on the 10° beam line occurred in the mid-fourth quarter of FY13. The deionized water in the target vessel was circulated at 40 mL/min through the TSML glovebox during the mini-SHINE experiments.

The turbidimeter controller demonstrated an error message once the beam line was at 60 Hz. In addition to the "E2010: light leak" error message on the controller display, the analog output from the controller went to –12 NTU. This error indicates that more light is hitting the two detectors inside the controller and is over-saturating the detector response. The hypothesis for this error was that additional light, similar to the 875 nm wavelength generated by the infrared LED source in the turbidimeter controller, was being produced within the fiberoptic cable. This excess light is thought to be luminescence or fluorescence produced by the interaction of high-energy x-rays, generated from the scraping of the electron beam at two of the stearing magnets and an aperature, with the quartz or quartz-dopants in the fiberoptic cable. Shielding of the fiberoptic cable run became apparent. Turbidity measurements for minSHINE runs 5 and 8 are shown in Figure 12.

Initially, two 0.75-in.-thick lead-sheet walls were installed to the right of the TSML box (Figure 13). The shielding was placed in this position to block x-rays being produced from an aperture and steering magnet located immediately before the beam line enters the mini-hot cell. This shielding proved ineffective during several more mini-SHINE water experiments. To better shield the fiberoptic cable, the cable was run through a 1-in. outer diameter (OD) steel conduit. The outside of the conduit was then wrapped in 1/8-in.-thick lead sheeting (Figure 14). This too proved ineffective; the light leak error re-occurred. Finally, a 1-in.-thick lead sheet wall was installed to shield the fiberoptic penetrations into the TSML glovebox from the beam line components up-field from the glovebox (Figure 15). This shielding configuration finally arrested the x-ray beams from interacting with the fiberoptic cable (Figure 16). As can be seen in Figure 16, the turbidity value did not go to the –12 NTU value as experienced during an "E2010: Light Leak" error message. A long-term test of the effectiveness of the additional shielding has not yet been performed. It is unknown at this time how stable the turbidity response will be to longer exposures during extended irradiation times.

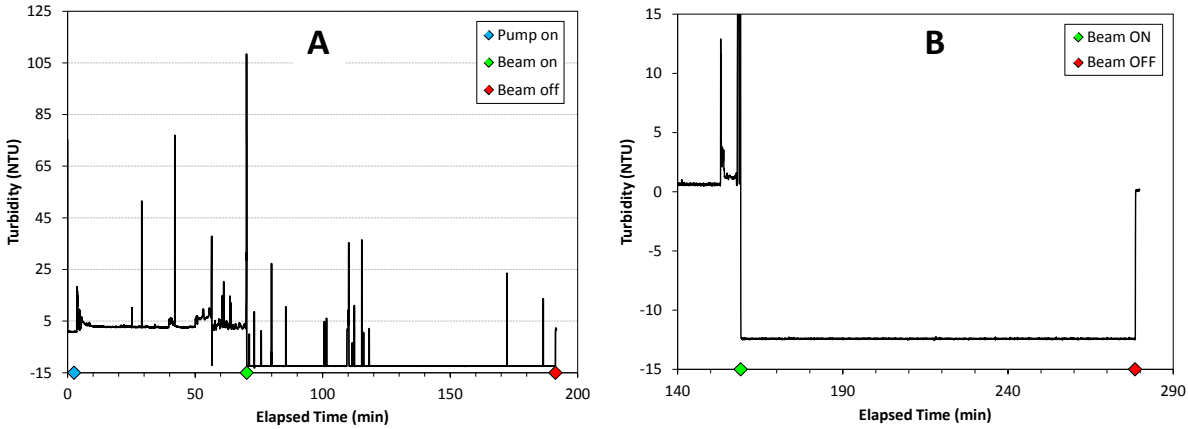

FIGURE 12 Response from the Kemtrak TC007 Turbidimeter Controller before, during, and after Operation of the Linac; Data from Micro-SHINE Irradiations 5 (A) and 8 (B), Conducted on 8/19/2013 and 9/11/2013, Respectively (An electron beam at 35 MeV, 60 Hz, and ~3.5 kW was directed down the 10° beam line toward the target solution vessel. The fiberoptic cable and the TSML glovebox were not shielded at this time.)

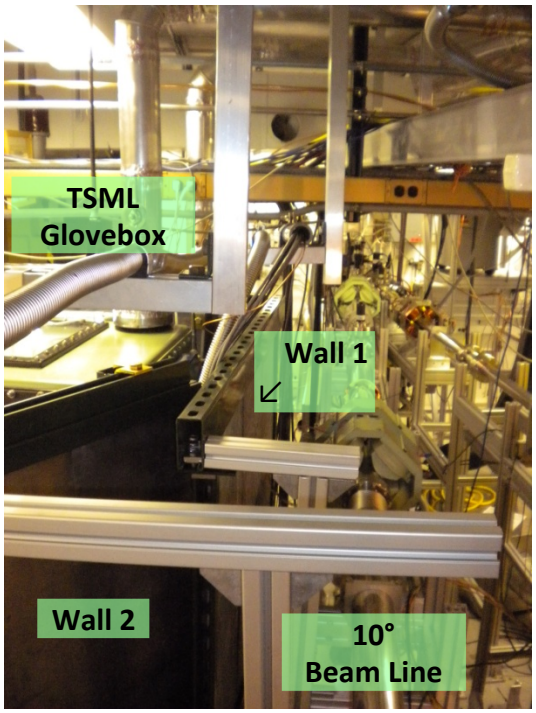

FIGURE 13 View from Mini-Hot Cell Looking Back along 10° Beam Line toward Pit/Cell 1 Separation Wall (The two 0.75-in.-thick lead sheet walls seen in photo are to the right of the TSML glovebox.)

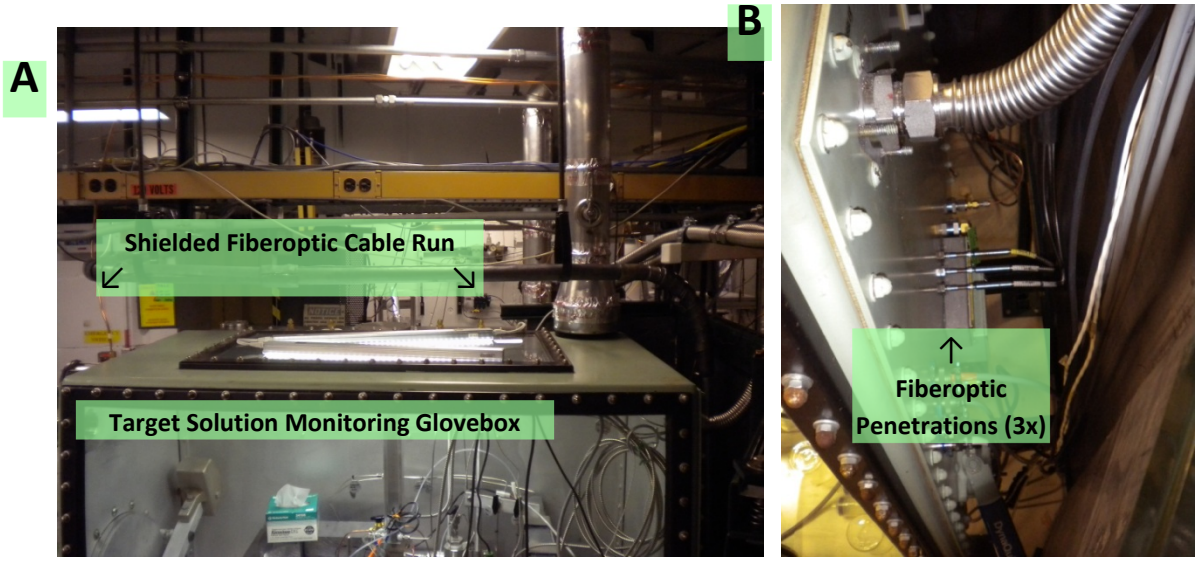

FIGURE 14 (A) 1-in. OD Steel Conduit Wrapped in 1/8-in.-Thick Lead Sheet That Houses the Fiberoptic Cable for the Turbidity Meter; (B) Fiberoptic Penetrations on the Right Side of the TSML Glovebox (The two 0.75-in.-thick lead sheet walls can be seen on the right side of photo [B].)

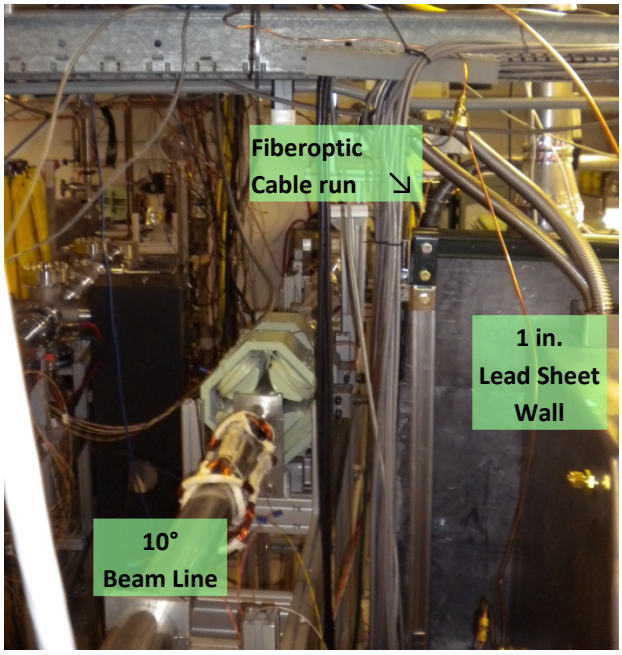

FIGURE 15 Photo Looking Down Range toward the Mini-Hot Cell That Houses the Target Vessel (The fiberoptic cable run over the target solution monitoring glovebox can be seen. Prior to installation of the 1-in.-thick lead sheet wall, the fiberoptic penetrations could be seen.)

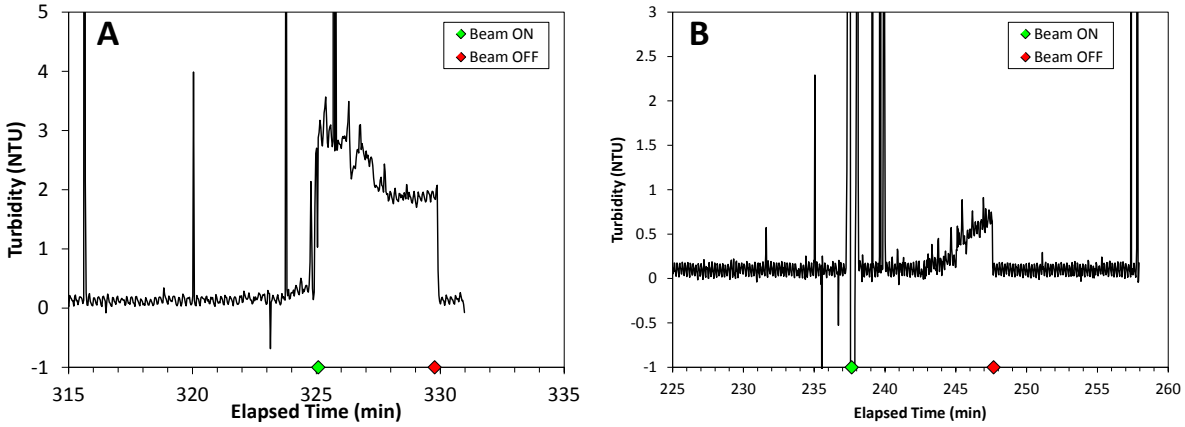

FIGURE 16 Response from the Kemtrak TC007 Turbidimeter Controller before, during, and after Operation of the Linac: an Electron Beam at 35 MeV, 60 Hz, and ~3.5 kW was Directed down (A) the 0° Beam Line to an Aluminum Beam Stop or (B) the 10° Beam Line toward the Target Solution Vessel (The fiberoptic cable is housed in 1-in. OD steel conduit that is wrapped with 1/8-in.-thick lead sheeting. Two 0.75-in.-thick lead sheet walls and a 1-in.-thick lead sheet wall shields the penetration of the fiberoptic cable through the right side of the TSML glovebox.)

3 GAS ANALYSIS RESULTS

Gas analysis results are shown for the first five water irradiations performed between July 26, 2013, and August 19, 2013. Each water irradiation lasted 2 h, and the final power achieved was 3.5 kW. During the experiments, 5 L of de-ionized water was irradiated by hitting a tantalum (Ta) target with the electron beam. The Ta target is inserted in a dry well in the center of the vessel. This produces neutrons and high-energy x-rays that cause radiolysis of the water. Radiolysis produces a host of radicals in the water that ultimately form peroxide, hydrogen, and oxygen.

The headspace gas of the vessel is analyzed using a Pfeiffer Prisma Plus Residual Gas Analyzer equipped with an SEM detector. A Shimadzu QP2010 gas chromatograph equipped with a TCD and a mass spectrometer (MS) is also used.

3.1 MINI-SHINE IRRADIATION 1

Data for this run are shown in Figure 17. The target solution was purged with helium several times to remove atmospheric gases from the vessel and solution. The system was purged for approximately 1.5 h. Residual nitrogen and oxygen remained in the system at concentrations of 300 and 100 ppm, respectively. Additional purging is required for each fresh solution. The atmospheric leak rate into the system is approximately 0.1% N_2/h and 0.05% O_2/h. The source of these leaks will be addressed later.

During this first water irradiation, the beam power was increased slowly. Initially, the power was set at 260 watts, and after 20 minutes, it reached 850 watts. The beam power was then increased to 1.78 kW at approximately 40 min, 2.86 kW at 55 min, and finally 3.5 kW at 60 min.

For the first 17 min of the run, only pre-catalyst gas sampling was performed. During the catalyst bypass test, a steady increase in hydrogen concentration during irradiation was observed, and oxygen concentration dropped at 33 min, which coincided with an increase in beam power (1.78 kW). Then at 49 min, oxygen levels dropped to ND, “not detectable.” These data were corroborated by GC-TCD analysis. Since the GC-TCD is less sensitive than the RGA for hydrogen analysis, it was not detected early in the experiment.

The beam-off time, at 95 min, coincided with the return of oxygen species momentarily. There was also a slight increase in the nitrogen signal. Within 18 min of the beam being off, oxygen appeared and increased rapidly. Hydrogen continued to rise to a maximum of 0.5%. As oxygen returned to the system, the hydrogen concentration began to decrease, as expected, due to catalytic recombination.

The post-irradiation rapid increase of nitrogen and oxygen is an interesting effect. A possible explanation is that during irradiation, there is localized pressure inside the vessel compared to the rest of the system, which can prevent diffusion into the vessel. The vessel is

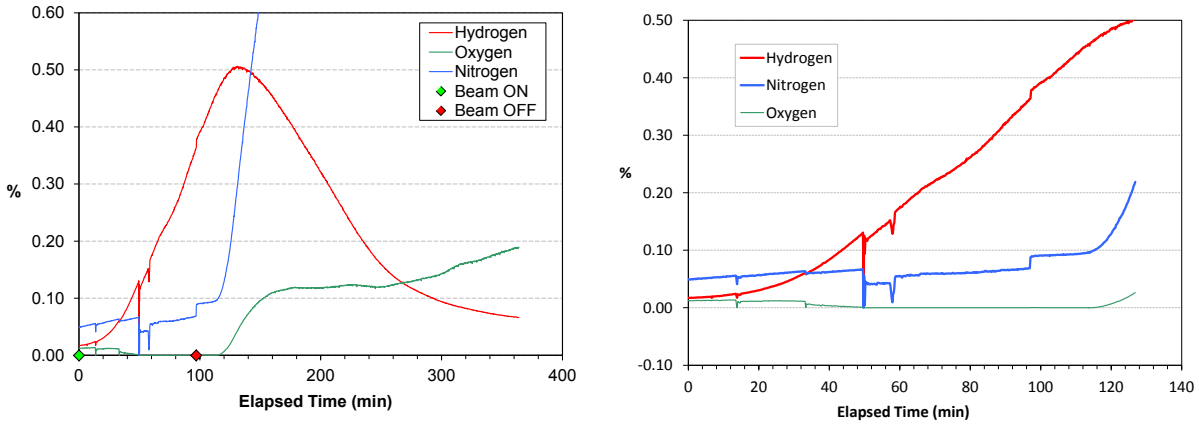

FIGURE 17 RGA Data from Mini-SHINE Experiment 1 with Water in Target Vessel

connected to the rest of the system by a long piece of 0.25-in. tubing. The source of nitrogen and oxygen in the form of leaks is almost 20 ft away.

Another strange observation is the drop in signal as the power increases. This requires further investigation, but a possible resolution may be to add more shielding.

3.2 MINI-SHINE IRRADIATION 2

For this irradiation (Figure 18), the beam power was at 3.5 kW during the entire irradiation. Prior to the beam hitting the target, the RGA showed signs of instability where analytes would disappear for short periods of time. Then, at approximately 35 min into the irradiation, the erratic behavior increased and the instrument shut itself down. At this time, the beam was turned off.

The RGA was restarted, and the beam was back on the target 14 min later. The lag time between the initial startup and the restart allowed for a considerable amount of atmospheric gases to leak into the system.

Only pre-catalyst sampling was performed during this experiment. With the headspace gases continuously being passed through the catalytic converter, hydrogen levels remained fairly constant throughout the experiment. Similar behavior of the analytes occurred during this experiment. When the beam was turned off, nitrogen, oxygen, and hydrogen increased at a more rapid rate then when the beam was on. GC-TCD analysis data corroborate well with the RGA data.

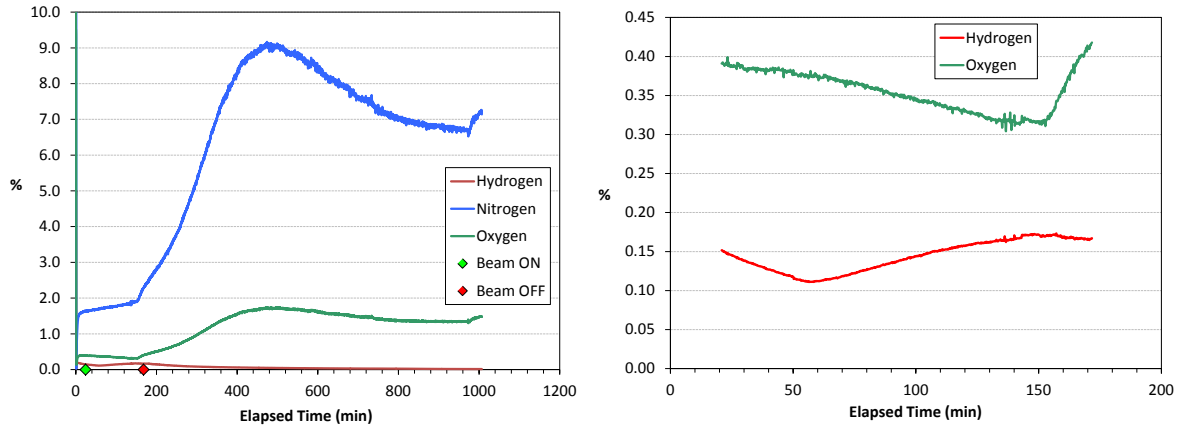

FIGURE 18 RGA Data from Mini-SHINE Experiment 2 with Water in the Target Vessel

3.3 MINI-SHINE IRRADIATION 3

During beam tune up, the RGA malfunctioned and needed to be restarted. The third irradiation (Figure 19) showed gas behavior relatively similar to that observed during irradiations 1 and 2, with one main difference. Hydrogen production was much lower for this run, which may be due to the use of deionized water for the irradiations. Ions in solution are known to affect the production of hydrogen and oxygen in a system. Even a slight difference in ion concentration, possibly due to the fact that the solubility limits of the system components had been reached during previous runs, affect how the two species are produced. All other data are corroborated by GC-TCD data. Hydrogen was less than the minimum detectable limits for the TCD.

Initially, the catalyst bypass test was performed where the headspace gas in the solution vessel does not contact the catalyst, which recombines the hydrogen and oxygen. As expected, at 92 min hydrogen steadily increased during this test. At 131 min, it began to drop when the gases passed through the catalyst. Then hydrogen began to steadily rise again at 140 min when the catalyst was bypassed again. Oxygen concentration, on the other hand, continued to decrease even though the catalyst was bypassed. This behavior was confirmed with the GC-TCD data.

When comparing RGA data to GC-TCD data, a difference is observed for gas-component concentrations when the beam is on. This difference is not observed in the absence of the beam.

3.4 MINI-SHINE IRRADIATION 4

When the beam began hitting the target, the RGA malfunctioned. The RGA needed to be restarted, and more shielding was added at this time. During this experiment (Figure 20), the catalyst bypass test was performed during the entire experiment since it was evident from previous experiments that hydrogen would not build up very quickly.

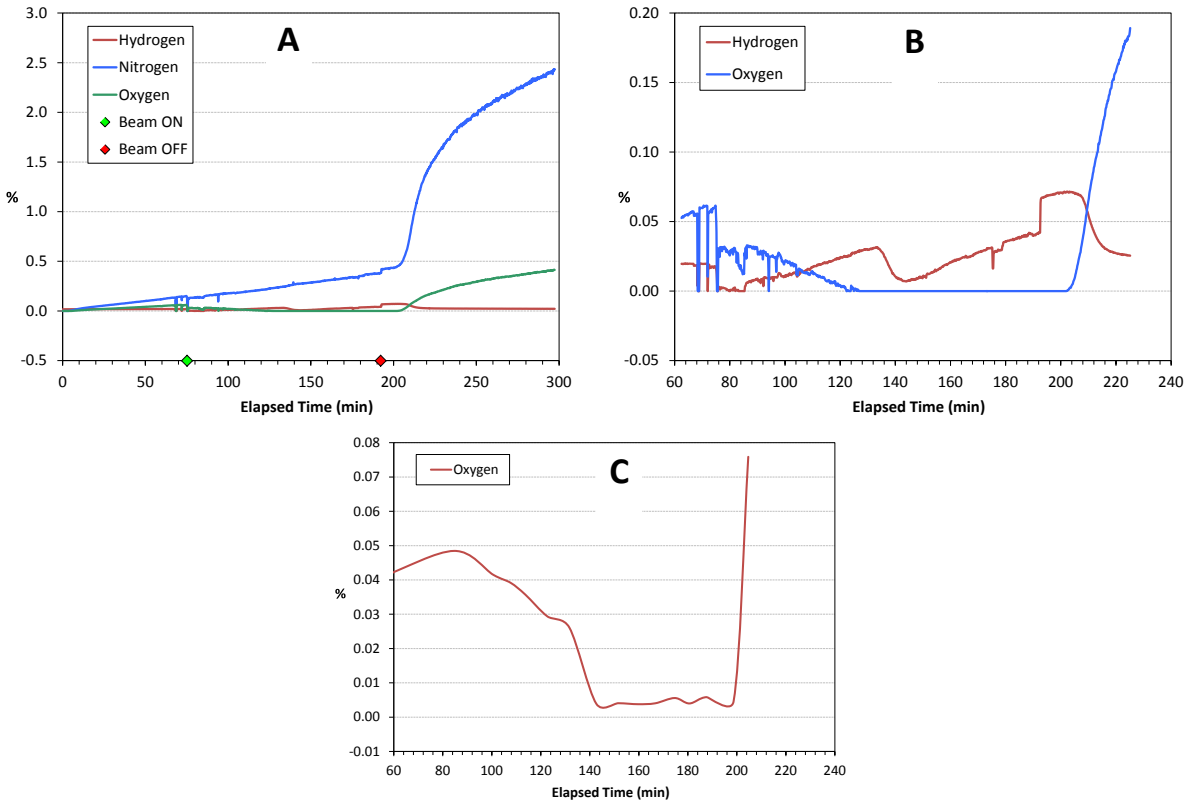

FIGURE 19 (A and B) RGA Data from Mini-SHINE Experiment 3 with Water in the Target Vessel; (C) Oxygen Concentration as Measured by GC-TCD

Hydrogen showed a linear increase, and oxygen was not detected during the entire experiment. The oxygen values were verified as not detectable by GC-TCD analysis. The hydrogen values were below the detection limits of the TCD.

3.5 MINI-SHINE IRRADIATION 5

Prior to this experiment, the leaks originating from the RGA exhaust were corrected. During the experiment (Figure 21), the chiller for the condenser on the gas analysis system failed. This appeared to cause analytical problems, mainly for the RGA. While all values were quite low, they appeared to be slightly erratic. Nitrogen data for the RGA were comparable to the GC-TCD data. The O_2 RGA values were measureable but near the detectable limit, while for the GC-TCD, they were not detected at the end of the experiment.

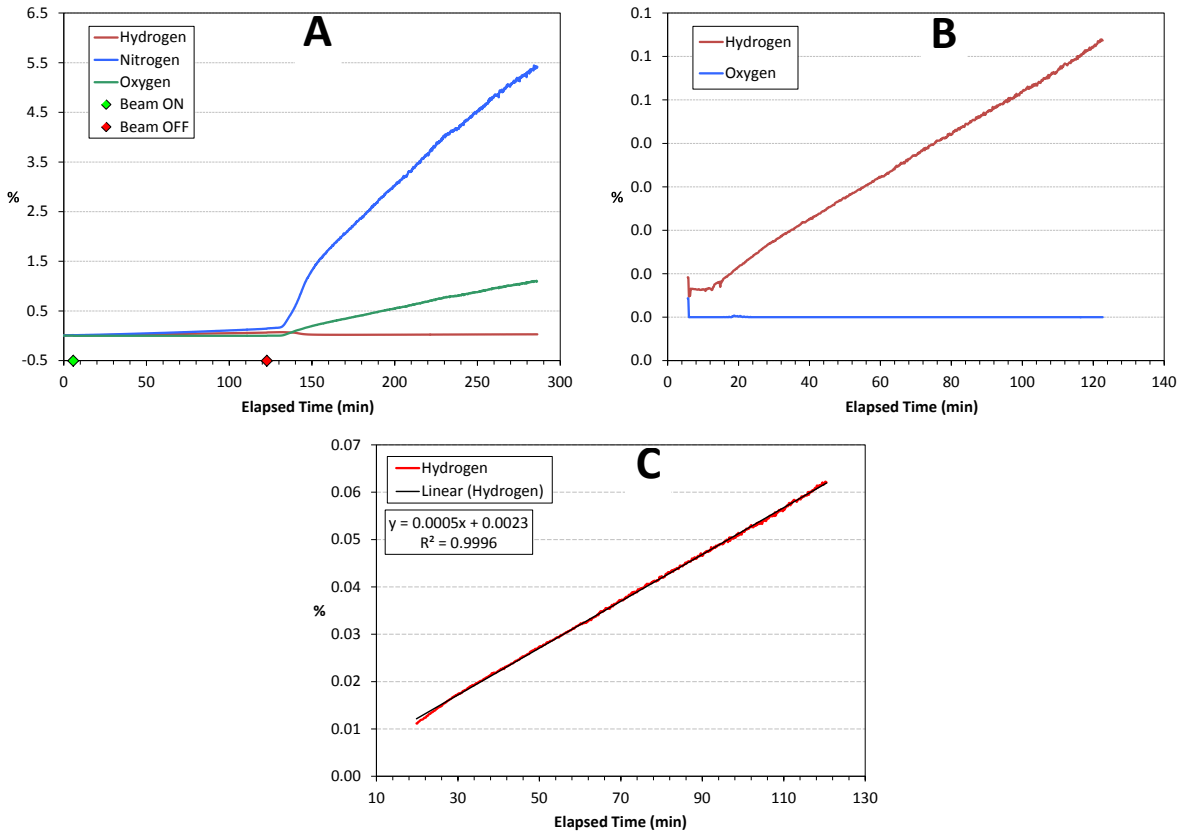

FIGURE 20 (A and B) RGA Data from Mini-SHINE Experiment 4 with Water in the Target Vessel; (C) Linearity of the Hydrogen Concentration during the Irradiation

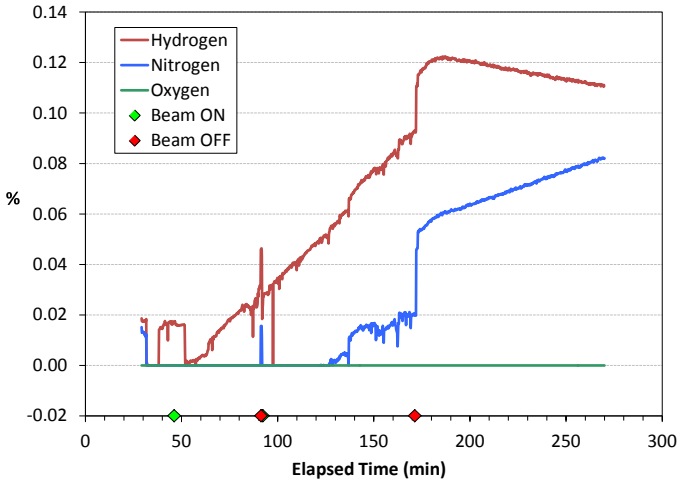

FIGURE 21 RGA Data from Mini-SHINE Experiment 5 with Water in the Target Vessel

4 MICRO-SHINE RESULTS

Micro-SHINE results showed that 1 ppm $FeSO_4$ is effective at catalyzing the destruction of H_2O_2 fast enough to prevent precipitation of uranyl peroxide. Interaction between the solutions and the Pt/alumina H_2:O_2 recombination catalyst caused large increases in pH post-irradiation and even precipitation for the samples from irradiations 2–6 between July 30, 2013, and August 20, 2013. The use of a stainless steel basket to hold the catalyst minimized interaction between the catalyst and solution. For samples irradiated between August 20, 2013 (second sample) and September 24, 13 (runs 6–9), the basket was used to hold the catalyst, and there was very little change in pH. Table 2 shows the pH values measured for all of the micro-SHINE salt solutions.

MKS Baratron manometer results (Table 3) show that the Pt/alumina recombination catalyst was very effective at recombining the H_2 and O_2 generated in the micro-SHINE samples. There was little to no pressure buildup in any of the samples. A mass of 0.8–1.0 g of Pt/alumina catalyst was effective at recombining the hydrogen and oxygen (3.5 g was used for samples irradiated between July 30, 2013, and August 19, 2013, runs 2–5). Pressure buildup was not measured in the samples irradiated on September 11, 2013 (8), and September 24, 2013 (9).

Gamma counting results are provided in Table 4 for the enriched uranium solutions irradiated on August 20, 2013 (6), and September 3, 2013 (7). The activities are based on what

TABLE 2 pH Values for Micro-SHINE Solutions Pre- and Post-Irradiation

Sample	Irradiation Date	Initial pH	Final pH
0.55 M $NaHSO_4$	07/30/13	1.00	–
1.26 M $NaNO_3$	07/30/13	1.00	–
130 g-U/L UO_2SO_4 – DU (10 ppm $FeSO_4$)	07/31/13	1.02	1.57
130 g-U/L UO_2SO_4 – DU (no H_2O_2 catalyst)	07/31/13	1.02	1.37
130 g-U/L UO_2SO_4 – LEU (1 ppm $FeSO_4$)	08/19/13	0.99	[a]
130 g-U/L UO_2SO_4 – LEU (10 ppm $FeSO_4$)	08/19/13	0.99	[a]
130 g-U/L UO_2SO_4 – LEU (1 ppm $FeSO_4$)[a]	08/20/13	0.96	1.17[b]
130 g-U/L UO_2SO_4 – LEU (1 ppm $FeSO_4$)	08/20/13	0.96	0.91
130 g-U/L UO_2SO_4 – HEU (1 ppm $FeSO_4$)	09/03/13	1.04	1.00
130 g-U/L $UO_2(NO_3)_2$ – HEU	09/03/13	1.00	1.00
130 g-U/L UO_2SO_4 (HEU) – 1 ppm Fe SO_4	09/11/13	1.04	0.99
130 g-U/L UO_2SO_4 (HEU) – 1 ppm Fe SO_4	09/11/13	1.04	1.02
130 g-U/L UO_2SO_4 (HEU) – 1 ppm Fe SO_4	09/24/13	1.04	1.05
130 g-U/L UO_2SO_4 (HEU) – 1 ppm Fe SO_4	09/24/13	1.04	1.03

[a] Solution came into contact with the Pt/alumina catalyst, and a precipitate formed. The pH values of these solutions with milky precipitates were 3.27 and 3.26. No precipitates were observed post-irradiation, but precipitation occurred after contact with the Pt/alumina catalyst.

[b] Solution came into contact with the Pt on alumina catalyst, and a significant amount of catalyst was found in the solution (new vial used for this sample).

TABLE 3 MKS Baratron Manometer Results for Micro-SHINE Samples Post-Irradiation

Sample	Irradiation Date	Before Needle Insertion (mbar)	After Needle Insertion (mbar)
H_2O	07/26/13	995.5	988.8
0.55 M $NaHSO_4$	07/30/13	996.4	995.4
1.26 M $NaNO_3$	07/30/13	995.4	993.9
130 g-U/L UO_2SO_4 – DU (10 ppm $FeSO_4$)	07/31/13	946.6	947.4
130 g-U/L UO_2SO_4 – DU (no H_2O_2 catalyst)	07/31/13	945.9	946.5
130 g-U/L UO_2SO_4 – LEU (1 ppm $FeSO_4$)	08/19/13	980.8	981.5
130 g-U/L UO_2SO_4 – LEU (10 ppm $FeSO_4$)	08/19/13	981.1	980.8
130 g-U/L UO_2SO_4 – LEU (1 ppm $FeSO_4$)	08/20/13	435.0	435.5
130 g-U/L UO_2SO_4 – LEU (1 ppm $FeSO_4$)	08/20/13	435.7	435.7
130 g-U/L UO_2SO_4 – HEU (1 ppm $FeSO_4$)	09/03/13	428.1	428.2
130 g-U/L $UO_2(NO_3)_2$ – HEU	09/03/13	428.3	426.8

TABLE 4 Gamma Counting Results for Uranium Micro-SHINE Samples

Isotope	UO_2SO_4-LEU (μCi) Irradiated on 08/20/13	UO_2SO_4-LEU (μCi) Irradiated on 08/20/13	UO_2SO_4-HEU (μCi) Irradiated on 09/03/13	$UO_2(NO_3)_2$-HEU (μCi) Irradiated on 09/03/13
Mo-99	21.5	21.2	102.1	85.9
I-131	4.1	4.2	23.0	17.8
I-133	90.2	84.3	485.1	393.3
Ba-140	5.3	5.4	28.7	22.5
Ce-143	46.2	45.6	241.9	197.8
Zr-97	77.3	75.9	416.0	324.9
Sr-91	155.9	167.9	974.2	760.7
I-135	198.9	216.2	1176.5	941.6
Ru-103	0.8	0.8	4.5	3.7
Np-239	38.7	41.1	–	–

was produced immediately after irradiation. Samples were gamma counted approximately 14 h post-irradiation. Samples were counted for 3 days; the amount of each isotope that was produced is based on results from two separate days, where dead times averaged 10% or less. Kr or Xe isotopes could not be clearly identified due to interference from other fission products. Only isotopes with clean peaks and correct decay values over the course of 3 days have been reported here. Gamma counting results are available for other samples but show comparable fission product inventories based on enrichment and radiation time.

5 MICRO-SHINE TRACER COLUMN RESULTS

The HEU uranyl-sulfate sample containing 1 ppm $FeSO_4$ irradiated on September 3, 2013 (7), was used as a spike for a depleted uranyl-sulfate solution containing 0.003 mM stable Mo, added as Na_2MoO_4. A 0.66-cm-ID × 3-cm-long column was packed with a pure titania sorbent made up of 110-μm particles with 60-Å pores. Approximately 260 mL of a uranyl sulfate solution containing an irradiated highly enriched uranium (HEU) micro-SHINE solution (2 mL) and 0.003 mM stable Mo was passed through the column in 2 h. After the feed solution was loaded onto the column at a flow rate of 2.2 mL/min, the column was washed with 10 column volumes (CV) of 0.1 M H_2SO_4 and 10 CVs of H_2O in the up-flow direction. The column and all solutions were heated to 80° C. Mo was recovered by passing 30 CVs of 0.1 M NaOH at 1 mL/min through the column in the down-flow direction. Table 5 shows the gamma counting results for the fission products that had clean peaks and showed accurate decay patterns over a period of 3 days for the various streams. Gamma counting results are ±5%, and the majority of Mo-99 was recovered in strips 2 and 3, which indicates that less than 30 CVs of 0.1 M NaOH is required to achieve a high Mo-recovery yield. Mo-recovery is highly dependent on pH, and once the column reaches a pH greater than 10, Mo elutes fairly quickly (~100% in 13 CVs). These data show that less volume is needed for entry into the concentration column operation, which will take less time for entry into the low-enriched uranium (LEU)-modified Cintichem purification process. It is important to note that these data also indicate that Mo(VI) has not been reduced to Mo(IV) or Mo(V) under the micro-SHINE irradiation conditions because all Mo adsorbed on the titania column and was easily recovered using 0.1 M NaOH. A significant amount of Zr (~65%) remained adsorbed on the column along with about half of the iodine, which is consistent with previous tracer tests performed using the same titania sorbent. One surprising result is the fact that Te-132 did not adsorb on the titania column; this contradicts previous tracer test results that showed that Te adsorbs as well as Mo on the titania sorbent. The irradiation environment may have changed Te's chemistry, removing its ability to adsorb on titania.

The column effluent was then treated with a mixture of $Ba(NO_3)_2$ and $Sr(NO_3)_2$ to convert the uranyl sulfate solution to a uranyl nitrate solution. These results are discussed in the report entitled *FY-13 Progress Report on the Cleanup of Irradiated 130 g-U/L Uranyl Sulfate SHINE Target Solutions*.

TABLE 5 Gamma Counting Results for the Micro-SHINE Tracer Column Experiment (% in each Stream)

Stream	Sr-91	Zr-97	Mo-99	Ru-103	Rh-105	I-131	Te-132	I-133	Ba-140	Ce-141	Ce-143
Effluent	91	33	0	100	100	29	100	3	100	100	100
Acid Wash	–	2	–	–	–	–	–	–	–	–	–
Water Wash 1	–	–	–	–	–	–	–	–	–	–	–
Strip 1 (1–6 CVs)	–	–	–	–	–	–	–	–	–	–	–
Strip 2 (7–14 CVs)	–	0.2	83	–	–	4	–	17	–	–	–
Strip 3 (15–20 CVs)	–	–	18	–	–	8	–	16	–	–	–
Strip 4 (21–30 CVs)	–	–	2	–	–	–	–	11	–	–	–
Water Wash 2	–	–	–	–	–	–	–	–	–	–	–
Amount left on column	9	64.8	0	0	0	59	0	53	0	0	0

6 IODINE SPECIATION RESULTS FROM MICRO-SHINE SOLUTIONS

Two micro-SHINE solutions (HEU, 2 mL each) were irradiated on September 11, 2013 (run 8), at The linac for 2 h. Iodine-speciation results could not be performed until 8 days post-irradiation due to the late arrival of chemicals needed to perform the extractions and high dead times during gamma counting for the irradiated samples. As a result, I-131 was the only remaining iodine species to use as a marker for the speciation studies. Te-131m, a fission product generated during irradiation, has a half-life of 30 h and decays to I-131. Because Te-131m had been through almost 8 half-lives at the time of analysis, its effect on the strange results observed is minimal, but its effect would be much more significant for samples examined less than 24 h post-irradiation. Gamma counting results (±5% error) for the first set of iodine extractions are shown in Table 6, and the procedure for performing the iodine extractions can be found in Youker et al. (2012). The iodine speciation results performed 8 days post-irradiation are difficult to interpret because they were irradiated under the same conditions and analyses were performed at the same time, but the results are slightly different. In the sample irradiated in the near port, a significant amount of iodine (43%) remains adsorbed on the quartz vial after the irradiated solution is removed, while only 26% of the iodine irradiated in the far port remains adsorbed on the quartz vial after solution removal. Both samples showed that about 2% will adsorb on the Pt/Al_2O_3 catalyst. Another main difference is the amount of iodine that has volatilized, 43% for sample irradiated in the near port and 72% for sample irradiated in the far port. Yet, the makeup for the different iodine species present in solution is quite similar for the 2 samples where 9-16% is present as I_2, 8-12% is present as I^-, and the remaining 75-78% is present as IO_3^-. Because the samples were not analyzed until 8 days post-irradiation, the fact that iodine is volatile in acidic solution was reinforced. Ultimately, these results suggest that if irradiated solutions remain unprocessed for a significant amount of time, the amount of iodine in the gas phase increases significantly.

Another set of HEU uranyl-sulfate samples were irradiated for 15 min at the linac on September 24, 2013 (run 9). The iodine extractions were performed 19 h post-irradiation. Because Te-131m had not been through a single half-life, I-133 and I-135 were used to track the different iodine species. Gamma counting results (±5% error) are shown in Table 7. These results are more consistent among the two samples irradiated at the same time. For the sample irradiated in the near port, about 20% of the iodine remains adsorbed on the interior of the quartz vial, while about 15% remains on the interior of the quartz vial irradiated in the far port. Much less iodine had volatilized in these samples (~5%–10%) compared to 40%–70% for samples analyzed 8 days post-irradiation. In both samples, iodide is the main species present, which is consistent with results obtained from iodine extractions performed using solutions irradiated at the Argonne 3.0-MeV Van de Graaff accelerator (Youker et al. 2012). In addition, these results are more relevant to plant-scale conditions where solutions will be processed completely less than 24 h post-irradiation. If iodide proves to be the dominant species, the LEU-modified Cintichem process can easily remove it if it co-elutes with Mo during the initial recovery and concentration column processes.

TABLE 6 Iodine Speciation Results Performed 8 days Post-Irradiation Using I-131 as a Marker

Sample ID	% Left in Vial	% Adsorbed on Pt/Al_2O_3 Catalyst	% Volatile	% in Solution	% in Solution as I_2	% in Solution as I^-	% in Solution as IO_3^-
HEU – 09/11/13 – Near Port	43	2.3	42.7	12	8.8	12.2	74.6
HEU – 09/11/13 – Far Port	26.1	1.9	71.6	0.9	15.9	7.9	78.2

TABLE 7 Iodine Speciation Results Performed 19 h Post-Irradiation Using I-133 and I-135 as Markers

Sample ID	% Left in Vial	% Adsorbed on Pt/Al_2O_3 Catalyst	% Volatile	% in Solution	% in Solution as I_2	% in Solution as I^-	% in Solution as IO_3^-
HEU – 09/24/13 – Near Port (I-133)	19.6	3.4	4.1	72.9	3.4	92.3	0.5
HEU – 09/24/13 – Near Port (I-135)	18.3	2.5	6.1	73.1	2.1	88.4	1.6
HEU – 09/24/13 – Far Port (I-133)	16.6	3.2	9.7	70.5	3.1	88.7	4.8
HEU – 09/24/13 – Far Port (I-135)	15.8	1.4	11.8	71	1.2	93.6	1.5

7 CONCLUSIONS AND FUTURE WORK

The process-monitoring loop and gas-collection and gas-analysis systems have been successfully tested using 5 L of deionized water in the target vessel.

LabVIEW works very well for remotely operating the system and collecting data.

The proper amount of shielding has been installed in the proper location to prevent the turbidity probe from malfunctioning.

Micro-SHINE irradiations showed that 1 ppm $FeSO_4$ is an effective catalyst at destroying peroxide before uranyl peroxide is able to form a precipitate. The Pt/Al_2O_3 catalyst was able to recombine the hydrogen and oxygen generated in the micro-SHINE samples, and no pressure buildup was observed in the samples post-irradiation.

A Mo-recovery column experiment performed using an irradiated micro-SHINE solution as a spike showed good Mo adsorption and recovery.

Iodine speciation results indicate that the speciation changes significantly as the elapsed time increases post-irradiation. The number of volatile species increases by at least four 8 days post-irradiation. The iodine results for the samples analyzed 19 hours post-irradiation are consistent with the previously reported Van de Graaff irradiation results.

Five liters of sodium bisulfate spiked with 100 mCi of Mo-99 will be irradiated next. The solution will be passed through an initial Mo-recovery column, and samples will be collected during irradiation. These steps will be done remotely, but sample retrieval will be done manually. The Mo-product solution will be acidified and passed through a concentration column, and the final product from the concentration column will be purified using the LEU-modified Cintichem process. The concentration column and purification processes will be performed in a hot cell in linac facility using manipulators.

Phase-2 micro-SHINE irradiations will occur during the sodium bisulfate irradiations. In phase 2, micro-SHINE samples will be open to the gas collection and analysis system to measure hydrogen and oxygen and collect the radiolytic gases, which will provide important data about radiolysis-gas generation rates before the 5-L uranyl sulfate mini-SHINE irradiations begin.

During the 5-L uranyl sulfate irradiation, the stainless tubing used in the process-monitoring loop and gas-collection system will be gamma counted post-irradiation to look for fission gases such as iodine that may potentially adsorb. From the iodine speciation tests using micro-SHINE solutions, it was shown that 15%–40% iodine adsorbed on the quartz vial. Off-gas samples will be taken during experiments to be shipped to Pacific Northwest National Laboratory for analysis of fission gases.

8 REFERENCES

Carpenter, 2004, "Carpenter Stainless Type 430FR Solenoid Quality," May 26. Available at http://cartech.ides.com/datasheet.aspx?i=103&e=63&c=techart.

Youker, A.J., J.F. Krebs, A. Hebden, K. Quigley, D. Stepinski, and G.F. Vandegrift, 2012, *Van de Graaff Experiments: Mo Redox Chemistry and Iodine Speciation*. ANL/CSE-13/17, September 27.